Hindawi Publishing Corporation
Journal of Chemistry
Volume 2013, Article ID 948010, 10 pages
http://dx.doi.org/10.1155/2013/948010

Research Article

Influence of Pyrazine Ring Doping on the ^{15}N and ^{11}B NMR and Electronic Structure Parameters in Zigzag Boron Nitride Nanotube: A DFT Study

Sattar Arshadi, Ameneh Asghari, Hojatollah Raheimi, and Saboora Abedini

Department of Chemistry, Payame Noor University, P.O. Box 19395-4697, Iran

Correspondence should be addressed to Sattar Arshadi; chemistry_arshadi@yahoo.com

Received 24 June 2012; Accepted 18 November 2012

Academic Editor: André Silva Pimentel

Density functional theory (DFT) calculations have been performed to investigate the properties of the electronic structures of pyrazine-doped boron nitride nanotubes (PD-BNNTs). The structural forms were firstly optimized and then nuclear magnetic resonance (NMR) parameters have been calculated on the optimized structures. The chemical shielding isotropic (CS^I) and chemical shielding anisotropic (CS^A) parameters were calculated at the sites of ^{11}B and ^{15}N nuclei in structural forms of BNNT including the perfect (a) model and PD-BNNTs (b), (c), and (d) models. The results indicated that the changes are most significant for those nuclei placed in the nearest neighborhood of the pyrazine-doped ring. The changes of the electronic sites of the N atoms are also more significant than those of the B atoms. The difference of LUMO-HOMO gap for the perfect model was larger than the PD-BNNTs models. Also the atomic charge distribution of N and B atoms has been determined in nanotubes by natural bond orbital (NBO) analysis. All calculations were performed by the B3LYP method and 6-311G** basis set using Gaussian 98 package of program.

1. Introduction

The existence of tubular forms of matter with nanoscale diameters has opened an exciting field of research in science. Since the discovery of carbon fullerene C_{60} by Smalley et al. in 1985 and carbon nanotubes by Iijima in 1991, electronic and mechanical properties of carbon and noncarbon nanotubes have been investigated by various groups [1–4].

Boron nitride (BN) is the first candidate to replace carbon, because hexagonal-BN structure is quite similar to that of graphite. Boron nitride nanotubes (BNNTs) have attracted an enormous amount of attention [5–13] as a typical representative of III–V compound tubes, partially because they have the morphology of honeycomb analogous to carbon nanotubes (CNTs). It has been shown that BNNTs exhibit many interesting properties such as significant resistance to oxidation at high temperatures when compared to the carbon nanotubes [14–19].

Unlike CNTs, all BN nanotubes exhibit semiconducting behavior with a wide band gap which is almost independent of tubular diameter, chirality, and number of walls [6, 20]. Furthermore, in contrast to the nonpolar CNTs, slight positive charge of boron atom (B) and slight negative charge of nitrogen atom (N) increase the polarity and the ionicity of the BNNTs. Therefore, the BNNTs have been proposed as more proper materials than the CNTs for applications in the specific electronic and mechanical devices.

The structure of BNNTs was firstly predicted by theoretical calculations [7, 21]. In 1995, Chopra et al. [5] reported the production of multiwalled BNNTs using arc-discharge techniques. The other synthesis methods are laser-assisted technique [22, 23] using pyrolytically grown CNTs as templates to prepare BNNTs, using chemical vapor deposition (CVD) by Lourie et al. [24]. In 2001, Bengu and Marks proposed a new method to synthesize the single-walled BN nanotubes [25]. This new synthesis technique has made it possible to bring BN nanotubes into the nanotechnology applications.

Previous studies have indicated that the properties of the electronic structure of the BNNTs are influenced by

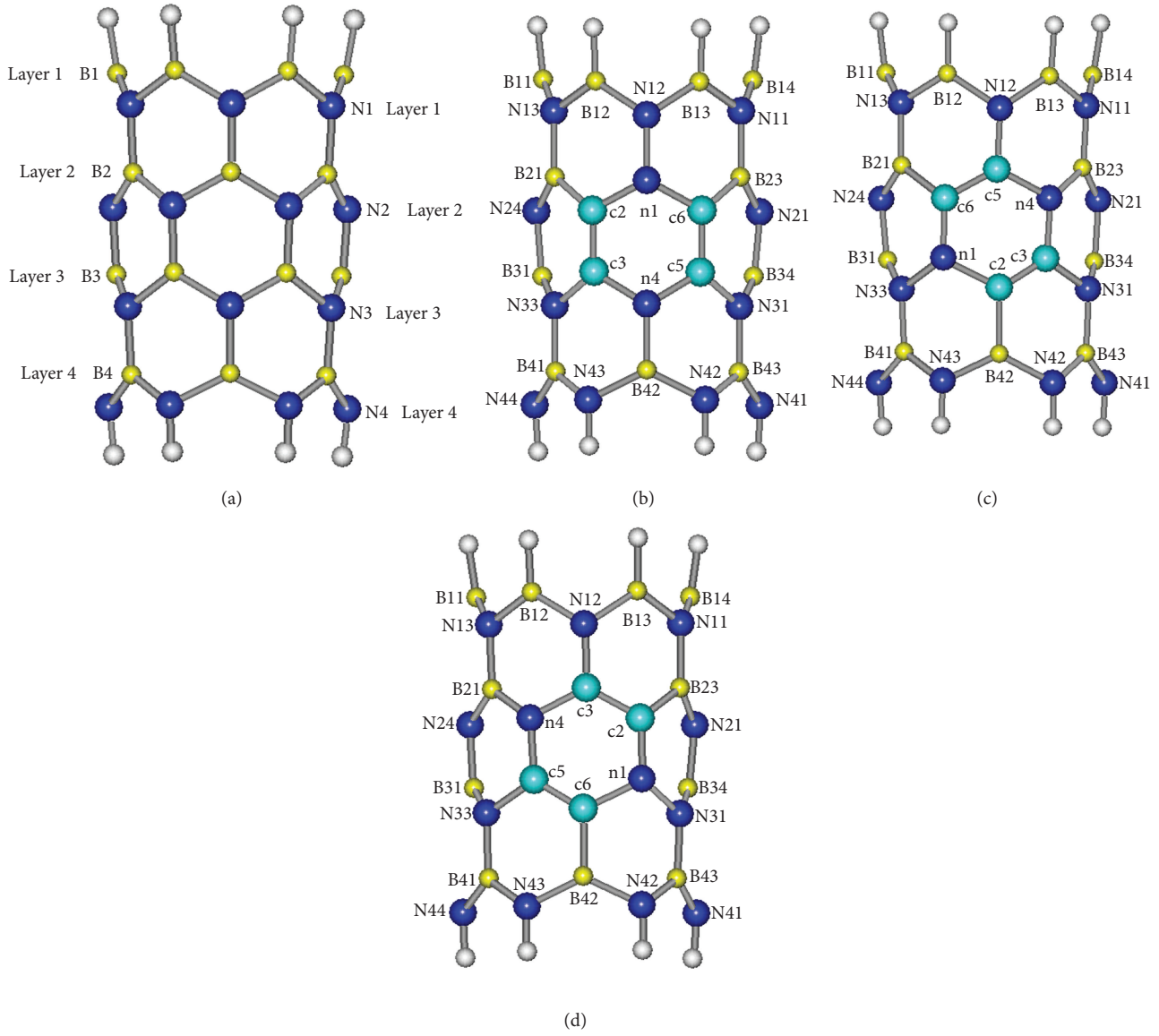

Figure 1: The front side view of perfect BNNTs model (a) and pyrazine-doped BNNTs models ((b)–(d)).

the doping atoms and impurities. Thus, uniformly doped BNNTs obtained through chemical modification could be very effective for tailoring the electronic properties, and the related mechanism and behavior are valuable to be explored in theory [26, 27].

Within present research, we have investigated the electronic structures and NMR parameters at the sites of ^{11}B and ^{15}N nuclei of perfect and pyrazine-doped models of BNNTs by density functional theory (DFT) calculations. Furthermore, we have investigated atomic charge distribution in nanotubes by natural bond orbital (NBO) [28] analysis.

2. Models and Computational Methods

Conveniently, BN nanotube could be presented by a (n, m) pair of numbers, where the (n, 0) and (n, n) BN nanotubes designate the zigzag and armchair types, respectively. For the zigzag type BN nanotube, n denotes the number of triazines in the circumference of the tube and the translation axis is the tubular length.

We have considered four models: a perfect and three pyrazine-doped models in Figures 1(a)–1(d) of the representative (6,0) zigzag single-walled BNNTs in present study. Figure 1(a) shows the perfect model, which consists of 24 boron (B) atoms and 24 nitrogen (N) atoms where the two tips of the nanotube are saturated by 12 hydrogen (H) atoms. In the perfect zigzag BNNTs, three B and three N atoms in the center of nanotube have been replaced by four carbon atoms (sp^2-hybridized) and two N atoms to create the pyrazine-doped BNNTs (pyrazine-BNNTs). Figures 1(b)–1(d) show three doped models which have different position for pyrazine ring in corresponding models.

Table 1: Structural energies, E_{LUMO}, E_{HOMO}, LUMO-HOMO gap, dipole moments and electronegativity for the perfect model (a) and PD-BNNT models ((b), (c), and (d)) at B3LYP/6-311G** level.

Models	Energy (keV)	E_{LUMO} (eV)	E_{HOMO} (eV)	$\Delta_{(LUMO-HOMO)}$ (eV)	Dipole moment (Debye)	Electronegativity (χ)
Perfect (a)	−52.22	−1.99	−6.85	4.86	7.47	4.42
(b)	−52.85	−1.86	−4.89	3.03	8.27	3.37
(c)	−52.85	−2.13	−4.70	2.57	6.93	3.41
(d)	−52.85	−2.13	−4.70	2.57	6.93	3.41

In the first step, the structures have been allowed to relax by all atomic geometrical optimization at the DFT level with B3LYP exchange-functional method and 6-311G** basis set. Furthermore NBO analysis was carried out on the B3LYP/6-311G** wave functions using version 3.1 of NBO package [29] included in Gaussian 98 program package [30].

Also we investigated electronegativity (χ) in the optimized structures. As we already know, electronegativities may be considered as the power of an atom in a given molecule to attract electrons to itself [31]. For an N-electron system with potential acting on an electron at r due to the nuclear attraction plus such other external forces as may be present (external potential) $\upsilon(r)$ and total energy E, electronegativity (χ) [32] is defined as the following:

$$\chi = -\left(\frac{\partial E}{\partial N}\right)_{\upsilon(r),T}. \quad (1)$$

The electronegativity is defined as the half part of the difference between the HOMO and the LUMO energies as follows:

$$\chi = \frac{-\left(E_{HOMO} + E_{LUMO}\right)}{2}. \quad (2)$$

The CS tensors are calculated for optimized nanotubes at the DFT level employing the B3LYP method and 6-311G** basis set based on the gauge independent atomic orbital (GIAO) approach [33]. The calculated CS tensors at the sites of ^{11}B and ^{15}N are yielded in the principal axes system (PAS) $\sigma_{33} > \sigma_{22} > \sigma_{11}$ [34]. Thereafter, they are converted to isotropic chemical shielding (CS^I) and anisotropic chemical shielding (CS^A) parameters using (3) [35] and are showed in Tables 5, 6, and 7:

$$CS^I\ (\text{ppm}) = \frac{\left(\sigma_{11} + \sigma_{22} + \sigma_{33}\right)}{3},$$
$$CS^A\ (\text{ppm}) = \frac{\sigma_{33} - \left(\sigma_{11} + \sigma_{22}\right)}{2}. \quad (3)$$

The DFT calculations have been performed by the Gaussian 98 package.

3. Results and Discussion

3.1. The Optimized Parameters. At the first step of this task, structural optimization was successfully carried out for the perfect ((a) model) and doped models ((b), (c), and (d) models) of the single-wall (6, 0) BNNT at the level of B3LYP, DFT method and 6-311G** basis set.

Subsequently, frequency calculations (keyword: FREQ = NORAMAN) were carried out by standard techniques on the optimized structures. For minimum state species, only real frequency values (with a positive sign) are accepted.

Table 1 presents the results for structural energies, the highest occupied molecular orbital (HOMO), the lowest unoccupied molecular orbital (LUMO), LUMO-HOMO gaps, dipole moments, and electronegativity (χ) obtained by the DFT calculations.

Our results indicated that the values of LUMO-HOMO gaps of the PD-BNNTs models are smaller than the perfect model. Also among the values of the LUMO-HOMO gaps of the pyrazine-doped models, the most significant changes were observed for the c and d models.

As we know, the band gap for the BN nanotube is higher in energy than the CNTs [6]. On the other hand, pyrazine-doped BN nanotube has similarities to CNTs in view of the prescience of carbons in the nanotube wall. Therefore the band gap in pyrazine-doped BN nanotube is similar to CNTs to some extent. This is proved by the calculated energies which are shown in Table 1.

The LUMO-HOMO gap is 4.86 eV for perfect model, 3.03 eV for (b) model, and 2.57 eV for (c) and (d) models, respectively (Table 1).

Also the densities of states (DOSs) of perfect and pyrazine-doped BNNT are shown in Figure 2 for better understanding the effect of pyrazine ring doping on the electronic structure of BNNT. It is clear that, after doping of pyrazine ring, the HOMO-LUMO energy gap of tube has significant change. On the other hand, the doping of pyrazine ring decreases the HOMO-LUMO energy gaps of the perfect BNNT.

The HOMO and LUMO in the perfect and pyrazine-doped models are plotted in Figure 3. For the perfect model, the HOMO is located on the nitrogen atoms of the (6, 0) zigzag BNNT model and corresponds to the lone pair of electron on nitrogen atoms. In contrast, the LUMO is uniformly distributed throughout the B–N bonds. For the pyrazine-doped models, the majority of the HOMO and LUMO are located at the pyrazine-doped regions.

The circumferences of the armchair BNNTs include both N and B atoms in both ends. In contrast to armchair models, circumferences of the zigzag BNNTs consist of one-type atoms, either N or B atoms; if one of the ends is formed by N atoms, the other end is formed by B atoms. The B atoms are slightly positive and the N atoms are slightly negative; therefore, the zigzag BNNT is a polar material that could be better seen by the value of dipole moment. Comparing the values of the dipole moments for the four models indicates

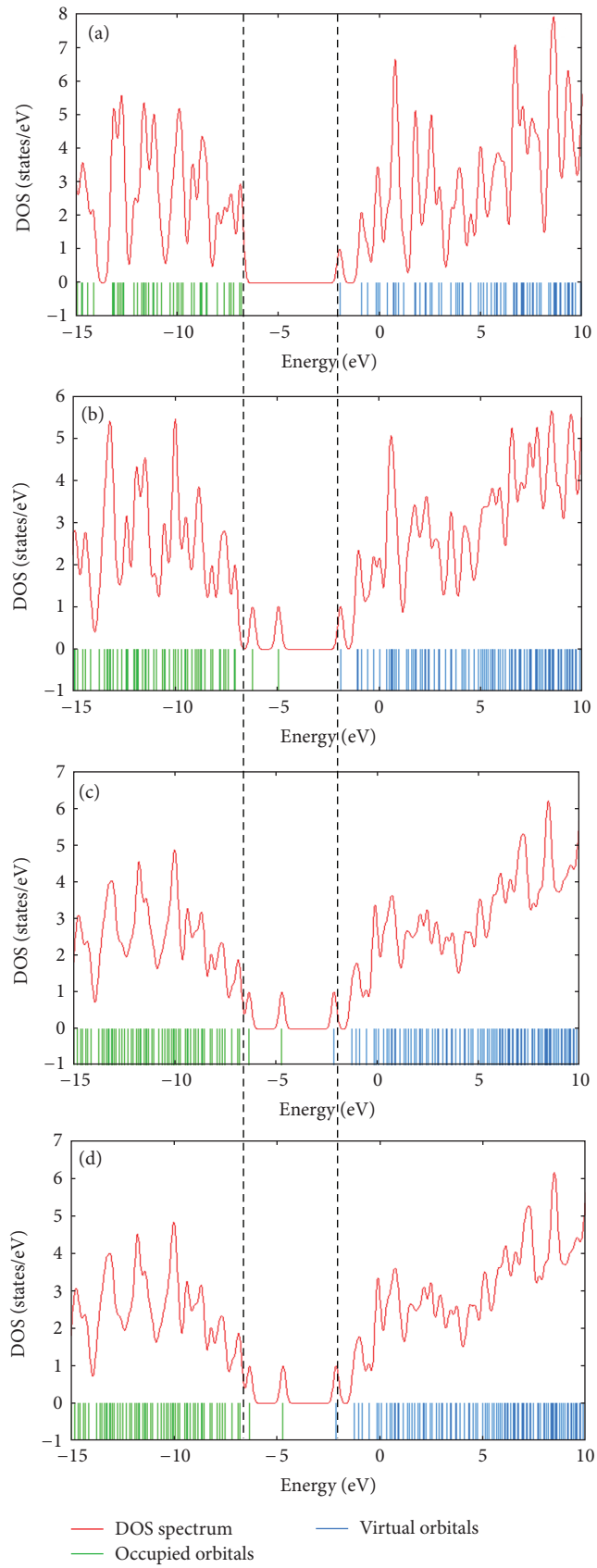

Figure 2: The density of states (DOS) of (a) the perfect model and (b), (c), and (d) pyrazine-doped models.

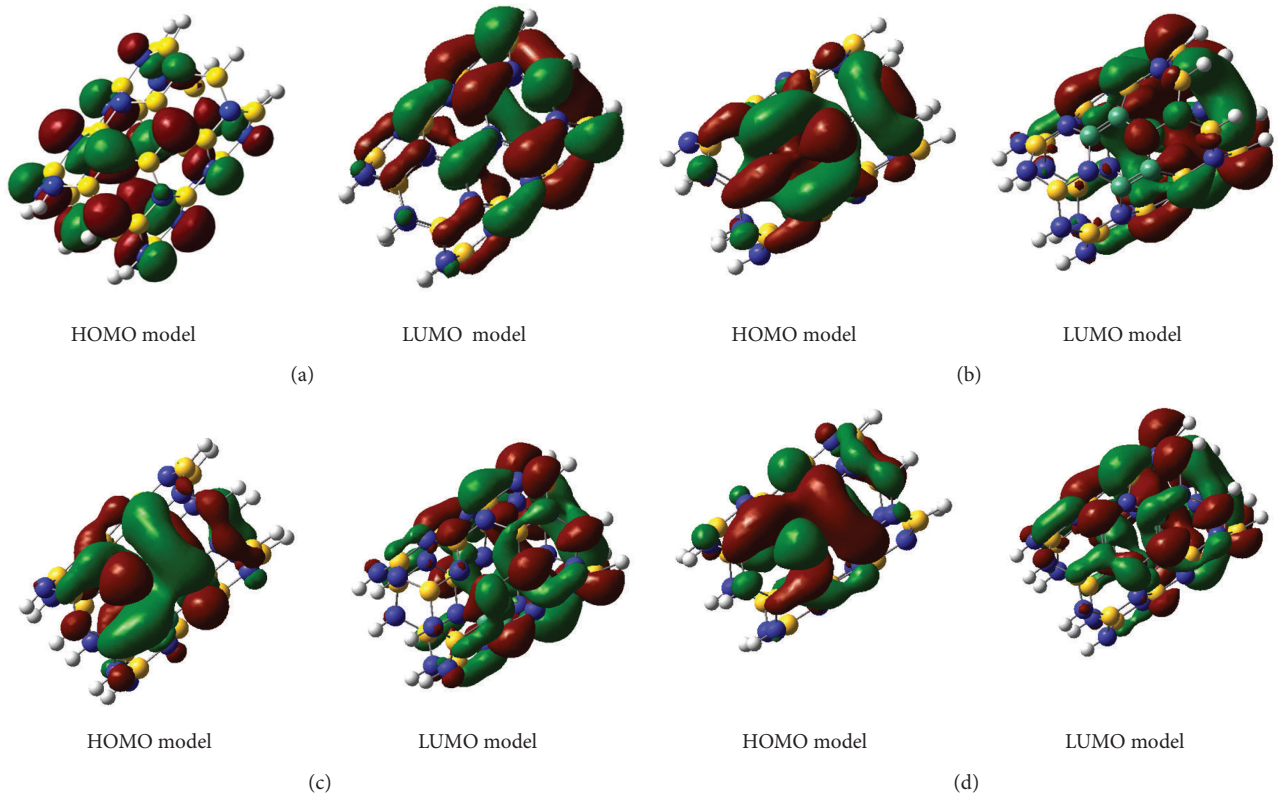

Figure 3: HOMO and LUMO orbitals for different models of the BNNTs: (a) perfect model, (b), (c), and (d) pyrazine-doped models.

Table 2: Optimized bond lengths (Å) and bond angles (°) for the perfect (in bracket) and PD-BNNT models (b) at B3LYP/6-311G** level.

Bonds	Length (Å)	Bonds	Length (Å)	Bonds	Length (Å)	Bonds	Angle (°)	Bonds	Angle (°)
B41–N44	1.45 [1.45]	B42–n4	1.44 [1.45]	B43–N41	1.45 [1.45]	c2–n1–c6	113 [118]	B23–c6–c5	119 [118]
B41–N33	1.45 [1.45]	B42–N42	1.45 [1.45]	c5–N31	1.42 [1.46]	c3–c2–n1	117 [118]	c5–N31–B43	119 [118]
B41–N43	1.45 [1.45]	c3–n4	1.43 [1.46]	B34–N31	1.46 [1.46]	c2–c3–n4	120 [120]	c3–n4–B42	119 [118]
B31–N33	1.46 [1.46]	c5–n4	1.43 [1.46]	c5–c6	1.35 [1.45]	c3–n4–c5	109 [111]	c5–n4–B42	119 [118]
c3–N33	1.42 [1.46]	c2–c3	1.35 [1.45]	c6–B23	1.54 [1.46]	n4–c5–c6	120 [120]	B41–N33–c3	119 [118]
B31–N24	1.44 [1.46]	c2–n1	1.44 [1.46]	B23–N11	1.43 [1.45]	c5–c6–n1	117 [118]	c3–N33–B31	115 [111]
B21–N24	1.45 [1.45]	n1–N12	1.42 [1.45]	B23–N21	1.45 [1.45]	B23–c6–n1	116 [110]	c5–N31–B34	115 [111]
B21–N13	1.43 [1.45]	C6–n1	1.44 [1.46]	B13–N11	1.46 [1.46]	B21–c2–n1	116 [110]	N24–B21–c2	117 [118]
c2–B21	1.54 [1.45]	B12–N12	1.46 [1.46]	B14–N11	1.46 [1.46]	B21–c2–c3	119 [118]	c6–B23–N21	117 [118]
B11–N13	1.46 [1.46]	B13–N12	1.46 [1.46]	B34–N21	1.44 [1.46]	n4–c5–N31	116 [118]	c6–B23–N11	119 [120]
B12–N13	1.46 [1.46]	B43–N42	1.45 [1.45]	B14–N16	1.46 [1.46]	N33–c3–n4	116 [118]	c2–B21–N13	119 [120]
B42–N43	1.45 [1.45]	B43–N31	1.45 [1.45]	B15–N16	1.46 [1.46]	c6–c5–N31	121 [120]	c2–c3–N33	121 [120]

that the value for the (b) model is significantly increased (D = 8.27 Debye) whereas those for the (c) and (d) models are significantly reduced (D = 6.93 Debye) compared with the perfect (a) model (D = 7.47 Debye), which means that the strengths of the charge points are balanced in the two latter models (Table 1).

The calculated structural energies in Table 1 also indicate no difference between the three models of the PD-BNNTs (−52.85 keV). On the other hand, the (c) and (d) models are structural isomers of the (b) model.

Tables 2, 3, and 4 present the optimized parameters including the bond lengths and bond angle for four models of the investigated (6, 0) BNNT (Figures 1(a)–1(d)).

In the perfect BNNT (Figure 1(a)), the average B–N bond length was 1.45-1.46 Å, but this value also was changed by the pyrazine-doping in the PD-BNNT due to existence of B–C, C–N, N–N, and C=C bonds in addition to B–N one.

However, the effects of this deformation were significant just at the geometrical properties of the nearest atoms to the pyrazine-doped ring whereas those of other atoms almost

Table 3: Optimized bond lengths (Å) and bond angles (°) for the perfect (in bracket) and PD-BNNT models (c) at B3LYP/6-311G** level.

Bonds	Length (Å)	Bonds	Length (Å)	Bonds	Length (Å)	Bonds	Angle (°)	Bonds	Angle (°)
B41–N44	1.46 [1.45]	c2–B42	1.52 [1.45]	B43–N41	1.46 [1.45]	c6–c5–n4	121 [118]	B23–n4–c3	119 [118]
B41–N33	1.44 [1.45]	B42–N42	1.45 [1.45]	c3–N31	1.42 [1.46]	n1–c6–c5	121 [118]	c3–N31–B43	118 [118]
B41–N43	1.46 [1.45]	n1–c2	1.47 [1.46]	B34–N31	1.48 [1.46]	c6–n1–c2	115 [120]	n1–c2–B42	117 [118]
B31–N33	1.46 [1.46]	c2–c3	1.36 [1.46]	c3–n4	1.40 [1.45]	n1–c2–c3	120 [111]	c3–c2–B42	121 [118]
n1–N33	1.49 [1.46]	c6–n1	1.40 [1.45]	n4–B23	1.46 [1.46]	c2–c3–n4	122 [120]	B41–N33–n1	115 [118]
B31–N24	1.44 [1.46]	c5–c6	1.38 [1.46]	B23–N11	1.43 [1.45]	c3–n4–c5	115 [118]	n1–N33–B31	117 [111]
B21–N24	1.46 [1.45]	c5–N12	1.41 [1.45]	B23–N21	1.44 [1.45]	B23–n4–c5	114 [110]	c3–N31–B34	110 [111]
B21–N13	1.45 [1.45]	c5–n4	1.44 [1.46]	B13–N11	1.45 [1.46]	B21–c6–c5	107 [110]	N24–B21–c6	115 [118]
c6–B21	1.53 [1.45]	B12–N12	1.47 [1.46]	B14–N11	1.46 [1.46]	B21–c6–n1	123 [118]	n4–B23–N21	108 [118]
B11–N13	1.46 [1.46]	B13–N12	1.45 [1.46]	B34–N21	1.44 [1.46]	c2–c3–N31	120 [118]	n4–B23–N11	119 [120]
B12–N13	1.44 [1.46]	B43–N42	1.44 [1.45]	B14–N16	1.45 [1.46]	N33–n1–c2	106 [118]	c6–B21–N13	120 [120]
B42–N43	1.45 [1.45]	B43–N31	1.47 [1.45]	B15–N16	1.46 [1.46]	n4–c3–N31	118 [120]	c6–n1–N33	114 [120]

Table 4: Optimized bond lengths (Å) and bond angles (°) for the perfect (in bracket) and PD-BNNT models (d) at B3LYP/6-311G** level.

Bonds	Length (Å)	Bonds	Length (Å)	Bonds	Length (Å)	Bonds	Angle (°)	Bonds	Angle (°)
B41–N44	1.46 [1.45]	c6–B42	1.52 [1.45]	B43–N41	1.46 [1.45]	n4–c3–c2	121 [118]	B23–c2–n1	123 [118]
B41–N33	1.47 [1.45]	B42–N42	1.45 [1.45]	n1–N31	1.49 [1.46]	c5–n4–c3	115 [118]	n1–N31–B43	115 [118]
B41–N43	1.44 [1.45]	c5–C6	1.36 [1.46]	B34–N31	1.46 [1.46]	n4–c5–c6	122 [120]	c5–c6–B42	121 [118]
B31–N33	1.48 [1.46]	c6–N1	1.47 [1.46]	n1–c6	1.47 [1.45]	c5–c6–n1	120 [111]	n1–c6–B42	117 [118]
c5–N33	1.42 [1.46]	c5–n4	1.40 [1.45]	c2–B23	1.53 [1.46]	c6–n1–c2	115 [120]	B41–N33–c5	117 [118]
B31–N24	1.44 [1.46]	c3–n4	1.44 [1.46]	B23–N11	1.45 [1.45]	n1–c2–c3	121 [118]	c5–N33–B31	110 [111]
B21–N24	1.44 [1.45]	c3–N12	1.41 [1.45]	B23–N21	1.46 [1.45]	B23–c2–c3	107 [110]	n1–N31–B34	117 [111]
B21–N13	1.43 [1.45]	c2–c3	1.38 [1.46]	B13–N11	1.44 [1.46]	B21–n4–c3	114 [110]	N24–B21–n4	118 [118]
n4–B21	1.46 [1.45]	B12–N12	1.45 [1.46]	B14–N11	1.46 [1.46]	B21–n4–c5	119 [118]	c2–B23–N21	115 [118]
B11–N13	1.46 [1.46]	B13–N12	1.47 [1.46]	B34–N21	1.44 [1.46]	c6–n1–N31	106 [118]	c2–B23–N11	120 [120]
B12–N13	1.45 [1.46]	B43–N42	1.46 [1.45]	B14–N16	1.46 [1.46]	N33–c5–c6	120 [118]	n4–B21–N13	119 [120]
B42–N43	1.45 [1.45]	B43–N31	1.44 [1.45]	B15–N16	1.45 [1.46]	c2–n1–N31	114 [120]	n4–c5–N33	118 [120]

remained unchanged. Furthermore, the changes of the bond angles were more than those of the bond lengths in the zigzag PD-BNNT.

Among theoretical methods, natural bond orbital (NBO) analysis is a unique approach to the evaluation of the atomic charges. It is clear that the charges of N and B atoms in these structures are negative and positive, respectively. The charges of N and B atoms at the end of tubes are smaller than those of other ones. Moreover, the results of NBO analysis indicated that the atomic charge distribution in the pyrazine-doped models is different from the perfect model.

3.2. NMR Parameters. In this computational work, the CS tensors (CS^I and CS^A) for various ^{11}B and ^{15}N atoms are calculated to study the influence of pyrazine ring doping on the electronic structure properties of the (6, 0) BNNT.

In the following text, the calculated ^{11}B and ^{15}N NMR parameters for the perfect and the pyrazine-doped models of BNNT are discussed, respectively.

3.2.1. The Perfect Model. Tables 5, 6, and 7 present the calculated NMR parameters for various ^{11}B and ^{15}N nuclei in the perfect model of BNNT. This model includes 24 B and 24 N atoms, where the edges are saturated by 12 H atoms (Figure 1(a)).

A quick look at the results reveals that various ^{11}B and ^{15}N nuclei are divided into four layers along the nanotube length. The layers have equivalent calculated CS^I and CS^A parameters, which means that the nuclei in each layer have equivalent electrostatic properties around similar nuclei.

The nature of the valence shells of the N atoms, which have lone pair of electrons, and the B atoms, which have a lack of electrons, is different; therefore, different behavior of the CS properties is expected and is also observed for these atoms.

The values of NMR properties for the ^{11}B and ^{15}N nuclei of the perfect model indicate that the B-mouth (B1) has the smallest value of CS^I (^{11}B), 64 ppm, and the N-mouth (N4) has the largest value of CS^I (^{15}N), 148 ppm, among the other layers of nuclei.

Table 5: The B3LYP/6-311G** calculated NMR parameters of the perfect model and model (b) of PD-BNNT.

Nuclei	CS^I (ppm)		CS^A (ppm)		Nuclei	CS^I (ppm)		CS^A (ppm)	
	Perfect	Doped	Perfect	Doped		Perfect	Doped	Perfect	Doped
Layer 1					Layer 1				
B1	64	—	60	—	N1	75	—	242	—
B11	—	65	—	59	N11	—	89	—	257
B12	—	74	—	54	N12	—	28	—	194
B13	—	74	—	54	N13	—	89	—	257
B14	—	65	—	59	N14	—	73	—	244
B15	—	64	—	60	N15	—	73	—	238
B16	—	64	—	60	N16	—	73	—	244
Layer 2					Layer 2				
B2	69	—	43	—	N2	111	—	195	—
B21	—	69	—	55	N21	—	105	—	209
B22	—	—	—	—	N22	—	—	—	—
B23	—	69	—	55	N23	—	—	—	—
B24	—	70	—	44	N24	—	105	—	209
B25	—	69	—	44	N25	—	110	—	195
B26	—	70	—	44	N26	—	110	—	195
Layer 3					Layer 3				
B3	69	—	39	—	N3	115	—	187	—
B31	—	68	—	40	N31	—	115	—	124
B32	—	—	—	—	N32	—	101	—	92
B33	—	—	—	—	N33	—	115	—	124
B34	—	68	—	40	N34	—	115	—	188
B35	—	70	—	38	N35	—	113	—	187
B36	—	70	—	38	N36	—	115	—	188
Layer 4					Layer 4				
B4	70	—	46	—	N4	148	—	94	—
B41	—	74	—	39	N41	—	153	—	86
B42	—	77	—	44	N42	—	163	—	74
B43	—	74	—	39	N43	—	163	—	74
B44	—	71	—	44	N44	—	153	—	86
B45	—	69	—	46	N45	—	147	—	98
B46	—	71	—	44	N46	—	147	—	98

In contrast, the opposite behavior is observed for the values of CS^A: the B-mouth has the largest value of CS^A (^{11}B), 60 ppm, whereas the N-mouth has the smallest value of CS^A (^{15}N), 94 ppm, among the other layers of nuclei.

3.2.2. The PD-BNNT Models. In the doped models, three B and three N atoms are doped by four carbon atoms (sp^2-hybridized) and two N atoms to construct PD- BNNTs ((b), (c) and (d)) models of Figure 1.

Due to this doping, the CS tensors at the sites of ^{11}B and ^{15}N nuclei which are directly bonded to the pyrazine ring undergo significant changes among the other nuclei in comparison with the perfect model. Furthermore, the magnitude of changes of the CS tensors is more significant at the sites of ^{15}N nuclei than at those of ^{11}B nuclei.

Although the other not directly bonded B and N layers are influenced by the pyrazine-doped ring, due to the sensitivity of the CS tensors, they also undergo some minor changes in the doped model. Moreover, the CS tensors at the sites of those nuclei shown in Figures 1(b)–1(d) (front side) change while those at the other side (back side) do not undergo any significant changes and their NMR parameters remain unchanged as those of the perfect model.

For example, in the (b) model (Figure 1(b)), NMR parameters of B42 (directly bonded) and B41, B43 (indirectly) were influenced by the pyrazine-doping whereas those of B44, B45, and B46 undergo some minor changes.

The evaluated NMR parameters at the sites of ^{11}B and ^{15}N nuclei in the perfect and doped models are presented in Tables 5, 6, and 7. In the (b) model of the zigzag PD-BNNT (Figure 1(b)), B32, B33, N22, and N23 atoms are

Table 6: The B3LYP/6-311G** calculated NMR parameters of the perfect model and model (c) of PD-BNNT.

Nuclei	CS^I (ppm)		CS^A (ppm)		Nuclei	CS^I (ppm)		CS^A (ppm)	
	Perfect	Doped	Perfect	Doped		Perfect	Doped	Perfect	Doped
Layer 1					Layer 1				
B1	64	—	60	—	N1	75	—	242	—
B11	—	66	—	57	N11	—	88	—	241
B12	—	73	—	54	N12	—	59	—	224
B13	—	70	—	54	N13	—	76	—	263
B14	—	65	—	58	N14	—	75	—	245
B15	—	64	—	59	N15	—	74	—	243
B16	—	64	—	58	N16	—	74	—	242
Layer 2					Layer 2				
B2	69	—	43	—	N2	111	—	195	—
B21	—	75	—	49	N21	—	115	—	195
B22	—	—	—	—	N22	—	112	—	137
B23	—	74	—	42	N23	—	—	—	—
B24	—	68	—	45	N24	—	119	—	199
B25	—	69	—	43	N25	—	110	—	198
B26	—	70	—	44	N26	—	110	—	194
Layer 3					Layer 3				
B3	69	—	39	—	N3	115	—	187	—
B31	—	70	—	42	N31	—	114	—	136
B32	—	—	—	—	N32	—	—	—	—
B33	—	—	—	—	N33	—	64	—	97
B34	—	68	—	42	N34	—	113	—	182
B35	—	68	—	41	N35	—	115	—	188
B36	—	69	—	41	N36	—	113	—	184
Layer 4					Layer 4				
B4	70	—	46	—	N4	148	—	94	—
B41	—	74	—	44	N41	—	151	—	92
B42	—	70	—	57	N42	—	141	—	119
B43	—	70	—	47	N43	—	152	—	94
B44	—	70	—	45	N44	—	155	—	77
B45	—	70	—	45	N45	—	149	—	94
B46	—	70	—	45	N46	—	148	—	95

doped by the C atoms and B22 and N32 atoms are doped by the N atoms which yield B–C, C–N, N–N, and C=C bonds. The results indicated that the changes are most significant for those nuclei placed in the nearest neighborhood of the pyrazine-doped ring.

In the first layer, N12 has the smallest CS^I and CS^A values (28 and 194 ppm, resp.) among the remaining N atoms in this layer. Also the calculated results show that those N atoms (N41, N42, N43, and N44) have the largest CS^I values (153, 163, 163, and 153 ppm) but the smallest CS^A values (86, 74, 74, and 86 ppm) among all N atoms.

The changes in the values of the CS parameters for B12, B13, B41, B42, and B43 atoms are also notable (Table 5).

The doping of B22, B33, N23, and N32 atoms by the C atoms and the doping of B32 and N22 atoms by the N atoms take place in the (c) model of the zigzag PD-BNNT (Figure 1(c)) which yield B–C, C–N, N–N, and C=C bonds.

Among the B atoms of the (c) model, B21, B23, and B42 are directly bonded to the pyrazine ring; hence, their NMR parameters (CS^I or CS^A) detect some changes due to the pyrazine-doping. Moreover, the NMR parameters of atoms further away show minor changes.

The CS^I and CS^A values for the N nuclei in the (c) model are different from those values in the (b) model. However notable changes in the CS tensors are observed for all of the N atoms due to the direct and indirect effect of the pyrazine-doped ring (Table 6).

In the (d) model (Figure 1(d)), B22, B32, N22, and N32 atoms are doped by the C atoms and B33 and N23 atoms are doped by the N atoms.

Table 7: The B3LYP/6-311G** calculated NMR parameters of the perfect model and model (d) of PD-BNNT.

Nuclei	CS^I (PPm)		CS^A (PPm)		Nuclei	CS^I (PPm)		CS^A (PPm)	
	Perfect	Doped	Perfect	Doped		Perfect	Doped	Perfect	Doped
Layer 1					Layer 1				
B1	64	—	60	—	N1	75	—	242	—
B11	—	65	—	58	N11	—	76	—	263
B12	—	70	—	54	N12	—	59	—	224
B13	—	73	—	54	N13	—	88	—	241
B14	—	66	—	57	N14	—	74	—	242
B15	—	64	—	58	N15	—	74	—	243
B16	—	64	—	59	N16	—	75	—	245
Layer 2					Layer 2				
B2	69	—	43	—	N2	111	—	195	—
B21	—	74	—	42	N21	—	119	—	199
B22	—	—	—	—	N22	—	—	—	—
B23	—	75	—	49	N23	—	112	—	137
B24	—	70	—	44	N24	—	115	—	195
B25	—	69	—	43	N25	—	110	—	194
B26	—	68	—	45	N26	—	110	—	198
Layer 3					Layer 3				
B3	69	—	39	—	N3	115	—	187	—
B31	—	68	—	42	N31	—	64	—	97
B32	—	—	—	—	N32	—	—	—	—
B33	—	—	—	—	N33	—	114	—	136
B34	—	70	—	42	N34	—	113	—	184
B35	—	69	—	41	N35	—	115	—	188
B36	—	68	—	41	N36	—	113	—	182
Layer 4					Layer 4				
B4	70	—	46	—	N4	148	—	94	—
B41	—	70	—	47	N41	—	155	—	77
B42	—	70	—	57	N42	—	152	—	94
B43	—	74	—	44	N43	—	141	—	119
B44	—	70	—	45	N44	—	151	—	92
B45	—	70	—	45	N45	—	148	—	95
B46	—	70	—	45	N46	—	149	—	94

The NMR parameters at the sites of ^{11}B, ^{15}N nuclei in (d) model are quite similar with the (c) model (Tables 6 and 7).

4. Conclusion

We have investigated the properties of the electronic structure of the pyrazine-doping in the BNNTs by performing the DFT calculations. The geometries were optimized at the B3LYP/6-311G** level of theory. The structural energies, LUMO-HOMO gaps, dipole moments, and electronegativity (χ) for perfect model and doped models have been calculated. The results of the perfect and doped models reveal some remarkable trends.

First, the optimization process reveals that BN nanotube surface is not smooth like CNTs but the N nuclei were relaxed outward and the B nuclei were relaxed inward of the nanotubes surface. Second, the values of dipole moments and band gaps are changed in the pyrazine-doped models. Third, the average B–N bond length in the (6,0) perfect BNNT was 1.45-1.46 Å, but this value was changed in the PD-BNNTs. Fourth, in the perfect model, the NMR parameters can divide BNNT structure into equivalent layers in which the B-mouth (B1) has the smallest CS^I but the N-mouth (N4) has the largest CS^I among the B and N layers, respectively.

Fifth, the results indicated the changes of NMR parameters are significant just for those atoms placed in the nearest neighboring of the pyrazine-doped ring. Clearly, pyrazine ring doping effect is totally different from Carbon impurity effect on electrostatic properties of BNNTs [36].

References

[1] H. W. Kroto, J. R. Heath, S. C. O'Brien, R. F. Curl, and R. E. Smalley, "C60: buckminsterfullerene," *Nature*, vol. 318, no. 6042, pp. 162–163, 1985.

[2] R. W. Cahn, "Nanostructured materials," *Nature*, vol. 348, no. 6300, pp. 389–390, 1990.

[3] S. Iijima, "Helical microtubules of graphitic carbon," *Nature*, vol. 354, no. 6348, pp. 56–58, 1991.

[4] M. S. Dresselhaus, G. Dresselhaus, and P. C. Eklund, *Science of Fullerenes and Carbon Nanotubes*, Academic Press, San Diego, Calif, USA, 1996.

[5] N. G. Chopra, R. J. Luyken, K. Cherrey et al., "Boron nitride nanotubes," *Science*, vol. 269, no. 5226, pp. 966–967, 1995.

[6] X. Blase, A. Rubio, S. G. Louie, and M. L. Cohen, "Stability and band gap constancy of boron-nitride nanotubes," *Europhysics Letters*, vol. 28, pp. 335–340, 1994.

[7] A. Rubio, J. L. Corkill, and M. L. Cohen, "Quasiparticle band structures of short-period superlattices and ordered alloys of AlN and GaN," *Physical Review B*, vol. 49, no. 3, pp. 1952–1956, 1994.

[8] J. Yu, J. Ahn, S. F. Yoon et al., "Semiconducting boron carbonitride nanostructures: nanotubes and nanofibers," *Applied Physics Letters*, vol. 77, no. 13, pp. 1949–1951, 2000.

[9] D. Golberg, P. Dorozhkin, Y. Bando, M. Hasegawa, and Z. C. Dong, "Semiconducting B-C-N nanotubes with few layers," *Chemical Physics Letters*, vol. 359, pp. 220–228, 2002.

[10] W. Q. Han and A. Zettl, "Functionalized boron nitride nanotubes with a stannic oxide coating: a novel chemical route to full coverage," *Journal of the American Chemical Society*, vol. 125, no. 8, pp. 2062–2063, 2003.

[11] C. Tang, Y. Bando, Y. Huang et al., "Fluorination and electrical conductivity of BN nanotubes," *Journal of the American Chemical Society*, vol. 127, no. 18, pp. 6552–6553, 2005.

[12] H. J. Xiang, J. Yang, J. G. Hou, and Q. Zhu, "Are fluorinated boron nitride nanotubes n -type semiconductors?" *Applied Physics Letters*, vol. 87, no. 24, Article ID 243113, pp. 1–3, 2005.

[13] Y. Chen, L. T. Chadderton, J. F. Gerald, and J. S. Williams, "A solid-state process for formation of boron nitride nanotubes," *Applied Physics Letters*, vol. 74, no. 20, pp. 2960–2962, 1999.

[14] E. Hernández, C. Goze, P. Bernier, and A. Rubio, "Elastic properties of C and BxCyNz composite nanotubes," *Physical Review Letters*, vol. 80, no. 20, pp. 4502–4505, 1998.

[15] A. P. Suryavanshi, M. F. Yu, J. Wen, C. Tang, and Y. Bando, "Elastic modulus and resonance behavior of boron nitride nanotubes," *Applied Physics Letters*, vol. 84, no. 14, pp. 2527–2529, 2004.

[16] D. Golberg, Y. Bando, K. Kurashima, and T. Sato, "Synthesis and characterization of ropes made of BN multiwalled nanotubes," *Scripta Materialia*, vol. 44, no. 8-9, pp. 1561–1565, 2001.

[17] Y. Xiao, X. H. Yan, J. X. Cao, J. W. Ding, Y. L. Mao, and J. Xiang, "Specific heat and quantized thermal conductance of single-walled boron nitride nanotubes," *Physical Review B*, vol. 69, no. 20, Article ID 205415, 2004.

[18] C. W. Chang, W. Q. Han, and A. Zettl, "Thermal conductivity of B-C-N and BN nanotubes," *Applied Physics Letters*, vol. 86, pp. 173102–173103, 2005.

[19] W. Han, Y. Bando, K. Kurashima, and T. Sato, "Synthesis of boron nitride nanotubes from carbon nanotubes by a substitution reaction," *Applied Physics Letters*, vol. 73, no. 21, pp. 3085–3087, 1998.

[20] A. Loiseau, F. Willaime, N. Demoncy, G. Hug, and H. Pascard, "Boron nitride nanotubes with reduced numbers of layers synthesized by arc discharge," *Physical Review Letters*, vol. 76, no. 25, pp. 4737–4740, 1996.

[21] X. Blase, A. Rubio, S. G. Louie, and M. L. Cohen, "Quasiparticle band structure of bulk hexagonal boron nitride and related systems," *Physical Review B*, vol. 51, no. 11, pp. 6868–6875, 1995.

[22] D. Golberg, Y. Bando, M. Eremets, K. Takemura, K. Kurashima, and H. Yusa, "Nanotubes in boron nitride laser heated at high pressure," *Applied Physics Letters*, vol. 69, no. 14, pp. 2045–2047, 1996.

[23] D. Golberg, Y. Bando, M. Eremets et al., "Boron nitride nanotube growth defects and their annealing-out under electron irradiation," *Chemical Physics Letters*, vol. 279, no. 3-4, pp. 191–196, 1997.

[24] O. R. Lourie, C. R. Jones, B. M. Bartlett, P. C. Gibbons, R. S. Ruoff, and W. E. Buhro, "CVD growth of boron nitride nanotubes," *Chemistry of Materials*, vol. 12, no. 7, pp. 1808–1810, 2000.

[25] E. Bengu and L. D. Marks, "Single-walled BN nanostructures," *Physical Review Letters*, vol. 86, no. 11, pp. 2385–2387, 2001.

[26] M. Mirzaei and A. Nouri, "The Al-doped BN nanotubes: a DFT study," *Journal of Molecular Structure*, vol. 942, no. 1–3, pp. 83–87, 2010.

[27] M. Mirzaei, "Calculation of chemical shielding in C-doped zigzag BN nanotubes," *Monatshefte fur Chemie*, vol. 140, no. 11, pp. 1275–1278, 2009.

[28] A. E. Reed, L. A. Curtiss, and F. Weinhold, "Intermolecular interactions from a natural bond orbital, donor-acceptor viewpoint," *Chemical Reviews*, vol. 88, no. 6, pp. 899–926, 1988.

[29] D. E. Glendening, A. E. Reed, J. E. Carpenter, and F. Weinhold, NBO, Version 3. 1.

[30] M. J. Frisch, G. W. Trucks, H. B. Schlegel et al., *Gaussian 98*, Gaussian, Pittsburgh, Pa, USA, 1998.

[31] R. G. Parr and W. Yang, "Density functional approach to the frontier-electron theory of chemical reactivity," *Journal of the American Chemical Society*, vol. 106, no. 14, pp. 4049–4050, 1984.

[32] K. D. Sen and C. K. Jorgensen, *Electronegativity, Structure and Bonding*, Springer, New York, NY, USA, 1987.

[33] K. Wolinski, J. F. Hinton, and P. Pulay, "Efficient implementation of the gauge-independent atomic orbital method for NMR chemical shift calculations," *Journal of the American Chemical Society*, vol. 112, no. 23, pp. 8251–8260, 1990.

[34] R. S. Drago, *Physical Methods for Chemists*, Saunders College Publishing, Orlando, Fla, USA, 2nd edition, 1992.

[35] U. Haeberlen, *Advances in Magnetic Resonance*, Academic Press, New York, NY, USA, 1976, Edited by J.S. Waugh.

[36] M. Mirzaei, "The carbon-doped (4,4) boron nitride nanotube: a computational NMR approach," *Physica E*, vol. 41, no. 5, pp. 883–885, 2009.